Densities and Phase Equilibria of Aluminum Chloride–Sodium Chloride Melts. 2. Two-Liquid-Phase Region

Armand A. Fannin, Jr.,* Lowell A. King, David W. Seegmiller, and Harald A. Øye†

Frank J. Seiler Research Laboratory (Air Force Systems Command) and Department of Chemistry, United States Air Force Academy, Colorado 80840

The separation into two immiscible liquid phases of $AlCl_3$–NaCl binary melts was studied from ca. 190 to 348 °C. Melt densities and compositions at the point of phase separation were calculated from the expansion of liquids contained in dilatometric tubes. The mole fraction of $AlCl_3$ at phase separation varies from 0.806 at 193.7 °C to 0.777 at 348 °C. Empirical equations are given which express density and mole fraction of $AlCl_3$ at separation as functions of temperature, with overall standard deviations of 0.001 g cm^{-3} and 0.002, respectively. The thermodynamic implications of the phase separation are discussed. A phase diagram is given for the entire $AlCl_3$–NaCl binary system.

Mixtures of $AlCl_3$ and NaCl exhibit a region of liquid–liquid immiscibility at high $AlCl_3$ content. This report describes the temperature–composition–density behavior of $AlCl_3$–NaCl mixtures in the immiscibility region and is a continuation of our previously reported data on densities of $AlCl_3$–NaCl melts (*1*).

Experimental Section

Densities were calculated by first measuring the volumes of the two liquid phases and the gas phase, contained in sealed, thick-walled, borosilicate dilatometer tubes. The total enclosed volume and the i.d. of each tube were ca. 3.4 cm^3 and 0.55 cm, respectively. Each tube had an index mark etched on it. The tubes were calibrated in the manner described for tubes A–D of ref *2*.

The phase boundary between the two liquid layers was very nearly flat, and no meniscus corrections were made for this boundary in the calculation of either liquid-phase volume. A hemispherical meniscus existed between the upper liquid and gas phases at the lowest temperatures (*2*). This rather uniformly flattened with increasing temperature and exhibited no detectable curvature near the critical temperature of $AlCl_3$. Accordingly, meniscus corrections were applied to this phase by assuming a linear variation in the height of the meniscus curvature from hemispherical at the $AlCl_3$ triple point (193.7 °C (*3*)) to flat at the critical point (348 °C, see below).

Materials purifications and handling, sample preparation and loading, bath temperature control and measurement, and measurement of meniscus location all were done as described previously (*1*). The sample tubes were mounted on a platform which could be rotated in the vertical plane while the tubes remained submerged in the thermostated bath. Tube rotation was performed at each different measurement temperature to ensure thorough mixing and equilibrium phase compositions within each dilatometer. All volume calculations were corrected for thermal expansion of the Pyrex glassware.

Data

Individual tube and sample parameters are given in Table I. Phase volumes are given in Table II at each experimental temperature. The data in Table II were not all taken in the order listed; measurements were made with both ascending and descending temperatures. There was no observable hysteresis in the volumes.

Table I. Sample Parameters[a]

sample	X^0	v^0, cm^3	m_{AlCl_3}, g	m_{NaCl}, g
I	0.8630	3.50	2.379	0.1655
II	0.8781	3.26	2.204	0.1342
III	0.8794	3.54	2.362	0.1420
IV	0.8809	3.21	2.069	0.1226
V	0.8930	3.44	2.240	0.1176
VI	0.9010	3.39	2.360	0.1137
VII	0.9050	3.36	2.244	0.1033
VIII	0.9201	3.34	2.260	0.0861
IX	0.9302	3.40	2.292	0.0753
X	0.9488	3.44	2.172	0.0514

[a] Estimated uncertainty in mole fraction = ±0.0005. Estimated uncertainty in total volume = ±0.05 cm^3. Estimated uncertainty in mass of $AlCl_3$ = ±0.002 g. Estimated uncertainty in mass of NaCl = ±0.0005 g.

The volume of the lower, NaCl-containing liquid, v', did only decrease slightly with increasing temperature, while the other two volumes changed much more dramatically. The volume behavior of the upper liquid phase, v'', with rising temperature fell into two clearly distinguishable groups. For samples I–V ($X^0 \leq 0.893$) v'' gradually increased with temperature to approximately 340 °C and then rapidly dropped to zero; v'' was zero at 347.20 °C (sample I) to 347.60 °C (sample V). On the other hand, v'' in samples VI–X ($X^0 \geq 0.901$) similarly gradually increased with temperature to approximately 340 °C and then very sharply rose further before the phase boundary suddenly vanished. Corresponding opposite changes of the gas volumes, v''', were experienced for both groups of samples. The highest temperature at which an upper liquid phase could be seen was 347.91 °C (sample X, $X^0 = 0.949$). At 348.48 °C, no upper liquid phase was observable.

Calculation of the Liquid Density and the Phase Boundary

The most straightforward procedure for data analysis is first to solve simultaneously for the three phase densities from the relationship

$$\rho' v' + \rho'' v'' + \rho''' v''' - m_{tot} = 0 \qquad (1)$$

where

$$v''' = v_{tot} - v' - v'' \qquad (2)$$

This procedure is valid as a consequence of the Gibbs phase rule: the three densities depend only on temperature, and not on overall composition. The volumes given in Table II were linearly interpolated in temperature to preselected temperatures. A simultaneous least-squares fit of all 10 samples to ρ', ρ'', and ρ''' was made at each of the desired temperatures.

It was then possible to solve simultaneously for the weight fraction of $AlCl_3$ at these same temperatures in each liquid phase from eq 3, where the assumption was made that no

$$y' \rho' v' + y'' \rho'' v'' + \rho''' v''' - m_{AlCl_3} = 0 \qquad (3)$$

† Permanent Address: Institutt for Uorganisk Kjemi, Norges Tekniske Høgskole, Universitetet i Trondheim, 7034 Trondheim—NTH, Norway.

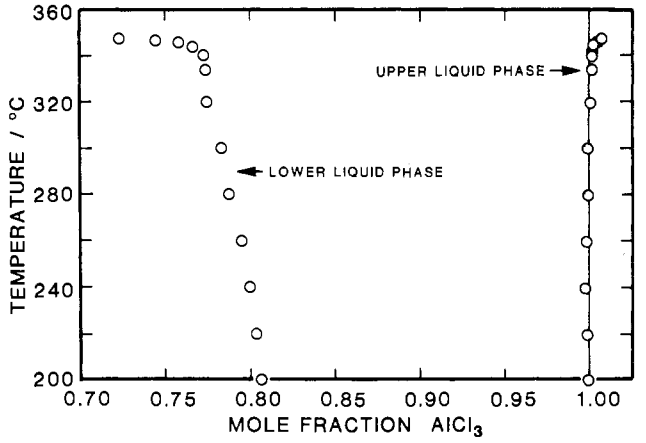

Figure 1. Mole fractions of liquid phases, calculated from simultaneously fitting all three phase densities.

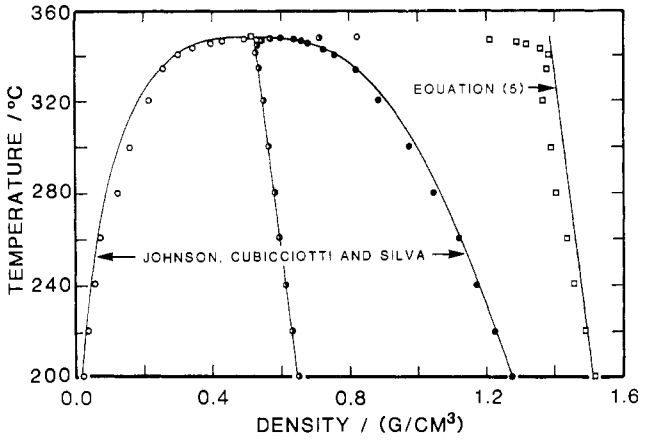

Figure 2. Densities of the two liquid phases and the gas phase. Individual points from preliminary calculation of densities from eq 1.

NaCl was present in the gas phase. A rough estimate of the pressure of gas molecules such as $NaAlCl_4$ or $Na_2Al_2Cl_6$ showed that the concentrations of these gas molecules indeed are negligible (10^{-5}%) above $AlCl_3$–NaCl melts with $X^0 = 0.8$ and $t = 300$ °C. Mole fractions were then calculated from weight fractions.

This procedure is not the best method for finding densities and mole fractions of the three phases, primarily because of the probability of large relative errors in mass being introduced into the low-density gas phase by the calculational method. Even so, two very important results came from this analysis. First, it was clear that virtually no NaCl was in the upper liquid layer. For 11 temperatures from 220 to 340 °C, inclusive, the calculated mean $X''' = 1.000 \pm 0.001$. Values of X' and X'' obtained by this procedure are shown in Figure 1.

The second observation was the appearance of typical $AlCl_3$ critical behavior at the highest temperatures. This can be seen clearly in Figure 2, in which are plotted the fitted values of ρ', ρ'', and ρ''' from eq 1. The apparently anomalous behavior of ρ' and ρ''' (Figure 2) and of X' and X''' (Figure 1) near the critical temperature should be ignored. This presumably is due to the profound influence of small volume errors in this region of very rapidly changing $AlCl_3$ liquid and vapor densities.

The critical temperature of $AlCl_3$ was found to be between 347.91 and 348.48 °C (see above). This is somewhat lower than we reported previously (*4*). The reason for the discrepancy is not clear.

Having established the absence of detectable NaCl in the upper liquid layer, we turned to a more suitable method for finding ρ' and X'. If ρ'' and ρ''' were available from independent measurements, eq 1 and 4 could be solved for ρ' and X' for each tube independently. Two extensive studies of ρ'' and ρ''' were published at about the same time (*4*, *5*) and yield virtually the same values of ρ'' and ρ''' at temperatures not too near the critical temperature. Johnson et al. (*5*) fitted their data to the Guggenheim relationship (slightly modified to reproduce their data better at low temperatures), which is flatter near their reported critical temperature of 620.2 K than a polynomial would predict (cf. ref *4*).

The solid lines in Figure 2 comprising the dome and rectilinear diameter were calculated from Johnson et al. (*5*). The ρ'' of Johnson et al. agree quite well with the ρ'' from our three-density fit, but, as suggested earlier, a large relative discrepancy exists in ρ'''. This discrepancy was reflected in a similarly sized absolute difference between ρ' calculated simultaneously with ρ'' and ρ''', and ρ' calculated independently of ρ'' and ρ'''. The latter ρ' is given by the solid line on the right side of Figure 2.

With the help of Figure 2, it is possible to understand the division into two categories of the behavior of v'' and v''' in the temperature range 340–348 °C. The grouping according to X^0, mentioned above, proved to be fortuitous. The phenomenon is related to the average density of liquid and gaseous $AlCl_3$ phases, i.e.

$$\rho_{av} = \frac{\rho''v'' + \rho'''v'''}{v'' + v'''} \qquad (4)$$

which in the present study lay between 0.44 and 0.58 g cm^{-3}.

In the temperature region 340–348 °C, the volume and the composition of the NaCl-containing phase change only slightly, while drastic changes in volume and density of the $AlCl_3$ liquid and gaseous phases occur as the top of the critical coexistence dome is approached. The two $AlCl_3$ phases can be considered to be an isolated system with constant total volume, $AlCl_3$ content, and average density (eq 4) in this temperature range. As a consequence of the lever rule, samples with $\rho_{av} < \rho_{crit} = 0.5185$ g cm^{-3} (*5*) must exhibit a sharp decrease in v'' and increase of v''' with increasing temperature, while the opposite behavior will occur for samples with $\rho_{av} > \rho_{crit}$. This is in accordance with our experimental findings: $\rho_{av} < 0.5158$ g cm^{-3} for samples I–V and $\rho_{av} > 0.5158$ g cm^{-3} for samples VI–X.

The critical temperature will only be found when $\rho_{av} = \rho_{crit}$, otherwise the temperature at which the third phase will disappear will be slightly lower than the critical temperature on either side of this density. We saw a tendency to this, but as the temperature variation for the disappearance of the third phase within the present ρ_{av} range was less than 1 °C, a reliable description of the top of the dome could not be achieved, other than that it was very flat.

Results and Discussion

For each of the ca. 300 experimental observations for which $t \leq 340$ °C, ρ'' and ρ''' were calculated from Johnson et al. (*5*) using 348 °C as the critical temperature, and ρ' was calculated from eq 1. These values of ρ' were then fitted to a straight line, given as eq 5. The standard deviation in ρ' was

$$\rho' = 1.6848 - (8.6844 \times 10^{-4})t \qquad (5)$$

0.001 g cm^{-3}. Equation 5 is plotted in Figure 2. Plots of v' vs. t show no noticeable deviations as they pass 340 °C or even at temperatures above the critical temperature. It appears that one can safely use eq 5 in the region from 340 to 348 °C. In Figure 3, densities are given for the complete single-liquid-phase region at selected temperatures from 200 to 340 °C. The diagram is bounded on the right by the separation into two liquid phases. The dashed lines are interpolated values between the results of our earlier study (*1*) and the present work. The points on the right were located from eq 5 and 6 (see below).

The mole fraction of the NaCl-containing phase, X', was calculated at each of the ca. 300 experimental points for which

Table II. Liquid Phase Volumes[a]

t, °C	v', cm³	v'', cm³	t, °C	v', cm³	v'', cm³
		Sample I			
192.8	1.130	0.621	274.6	1.109	0.753
193.3	1.130	0.624	282.4	1.095	0.769
197.7	1.137	0.620	289.4	1.090	0.787
197.9	1.134	0.621	297.1	1.087	0.793
202.7	1.127	0.633	304.0	1.079	0.806
202.8	1.130	0.632	311.7	1.074	0.817
203.6	1.135	0.629	318.6	1.063	0.827
207.8	1.130	0.635	325.8	1.056	0.834
207.8	1.135	0.632	328.1	1.061	0.821
213.0	1.138	0.642	332.8	1.041	0.827
219.1	1.134	0.652	335.8	1.049	0.804
219.2	1.134	0.652	340.1	1.041	0.775
226.9	1.136	0.662	341.9	1.041	0.746
232.9	1.130	0.677	344.9	1.032	0.634
238.4	1.129	0.685	345.4	1.038	0.604
244.2	1.126	0.694	345.5	1.032	0.593
248.9	1.127	0.699	346.7	1.032	0.430
255.0	1.128	0.708	346.7	1.034	0.398
260.2	1.118	0.725	347.1	1.034	0.289
267.4	1.113	0.740			
		Sample II			
192.7	0.920	0.709	274.6	0.904	0.840
193.2	0.917	0.704	282.4	0.887	0.860
197.7	0.916	0.705	289.4	0.885	0.876
197.9	0.920	0.706	297.0	0.886	0.885
202.8	0.915	0.718	304.0	0.879	0.899
202.8	0.919	0.716	311.7	0.872	0.915
203.5	0.925	0.713	318.6	0.862	0.933
207.8	0.914	0.725	325.8	0.859	0.943
207.8	0.925	0.720	328.1	0.862	0.933
213.0	0.922	0.731	332.8	0.852	0.949
219.1	0.925	0.736	335.8	0.855	0.938
219.2	0.923	0.738	340.1	0.844	0.935
226.8	0.921	0.749	341.9	0.849	0.918
232.9	0.922	0.759	345.4	0.842	0.845
238.4	0.917	0.773	345.4	0.842	0.840
244.2	0.917	0.781	346.6	0.844	0.758
248.9	0.917	0.788	346.7	0.844	0.742
255.0	0.912	0.799	347.0	0.840	0.670
260.2	0.909	0.813	347.2	0.843	0.416
		Sample III			
192.8	0.978	0.778	282.4	0.945	0.939
193.2	0.976	0.770	289.4	0.943	0.953
197.7	0.979	0.771	297.0	0.939	0.963
202.8	0.980	0.784	311.7	0.925	0.995
202.8	0.975	0.786	318.6	0.914	1.011
203.5	0.979	0.785	325.8	0.914	1.017
207.8	0.974	0.795	328.1	0.915	1.014
207.8	0.976	0.796	332.8	0.905	1.023
212.9	0.981	0.801	335.8	0.907	1.014
219.1	0.978	0.810	340.1	0.898	1.002
219.2	0.984	0.809	341.8	0.902	0.988
226.8	0.980	0.818	344.8	0.892	0.921
232.9	0.974	0.835	345.3	0.893	0.911
244.2	0.971	0.856	345.4	0.893	0.899
248.9	0.968	0.866	346.6	0.898	0.806
255.0	0.967	0.876	346.7	0.891	0.799
260.2	0.963	0.890	347.0	0.892	0.719
267.4	0.962	0.900	347.2	0.892	0.475
274.5	0.957	0.918			
		Sample IV			
194.9	0.862	0.670	281.1	0.825	0.812
202.2	0.859	0.683	287.0	0.822	0.823
209.6	0.857	0.690	292.0	0.820	0.829
219.6	0.858	0.704	295.8	0.815	0.836
234.5	0.849	0.731	301.2	0.817	0.841
236.6	0.845	0.733	305.7	0.810	0.854
239.2	0.856	0.727	310.0	0.808	0.859
241.7	0.850	0.738	315.0	0.805	0.863
242.9	0.847	0.746	319.8	0.804	0.865
244.2	0.844	0.750	324.8	0.800	0.871
246.5	0.847	0.748	330.8	0.798	0.873
251.6	0.847	0.761	334.6	0.796	0.864
256.6	0.837	0.796	344.3	0.779	0.772
261.6	0.837	0.777	346.5	0.783	0.560
266.4	0.836	0.789	346.8	0.784	0.476
271.1	0.836	0.792	346.9	0.774	0.350
276.1	0.829	0.805	347.2	0.779	0.156
		Sample V			
194.0	0.814	0.852	281.7	0.791	1.011
194.5	0.812	0.848	288.8	0.786	1.027
198.9	0.813	0.861	291.6	0.780	1.039
199.4	0.816	0.856	296.2	0.786	1.042
204.1	0.812	0.867	296.6	0.777	1.049
204.5	0.812	0.868	303.6	0.781	1.057
205.0	0.812	0.868	310.8	0.774	1.071
209.7	0.813	0.875	317.7	0.767	1.088
210.1	0.814	0.875	325.1	0.766	1.100
214.0	0.814	0.879	332.3	0.761	1.117
225.7	0.814	0.900	332.5	0.761	1.115
226.3	0.816	0.898	339.7	0.759	1.116
239.0	0.811	0.924	343.5	0.755	1.093
241.7	0.806	0.935	345.8	0.767	1.015
249.0	0.812	0.943	346.2	0.765	1.017
259.3	0.804	0.965	346.9	0.770	0.934
264.9	0.799	0.975	347.0	0.755	0.939
272.8	0.795	0.995	347.5	0.756	0.704
280.1	0.788	1.013			
		Sample VI			
194.9	0.809	0.954	281.2	0.778	1.153
202.2	0.811	0.966	286.8	0.774	1.172
209.6	0.811	0.975	292.2	0.767	1.196
219.6	0.802	1.007	295.7	0.767	1.203
234.5	0.801	1.031	300.9	0.763	1.219
236.6	0.802	1.030	305.6	0.762	1.235
239.0	0.787	1.051	309.8	0.760	1.250
241.7	0.786	1.049	315.0	0.764	1.264
242.9	0.795	1.046	319.8	0.760	1.286
244.2	0.798	1.051	324.8	0.757	1.307
246.2	0.794	1.061	327.4	0.747	1.328
251.6	0.798	1.070	330.8	0.745	1.349
256.5	0.790	1.078	334.6	0.740	1.373
261.6	0.789	1.099	344.3	0.735	1.513
266.5	0.787	1.111	346.5	0.733	1.665
270.9	0.786	1.121	346.8	0.735	1.741
276.2	0.784	1.138	347.0	0.729	1.856
		Sample VII			
193.9	0.715	0.964	283.8	0.699	1.153
194.6	0.714	0.959	288.8	0.702	1.157
198.9	0.716	0.971	291.7	0.692	1.178
199.4	0.716	0.969	296.2	0.700	1.178
204.1	0.721	0.974	296.6	0.691	1.181
204.5	0.716	0.979	303.6	0.692	1.204
205.1	0.718	0.979	310.8	0.689	1.226
209.8	0.716	0.987	317.8	0.687	1.251
210.0	0.713	0.986	325.1	0.682	1.278
213.8	0.718	0.994	332.3	0.675	1.316
226.3	0.719	1.015	332.4	0.678	1.311
239.1	0.718	1.041	339.8	0.670	1.358
241.8	0.714	1.049	343.5	0.670	1.395
249.0	0.714	1.065	345.8	0.683	1.436
259.2	0.713	1.086	346.2	0.682	1.453
265.0	0.711	1.098	346.9	0.686	1.487
272.8	0.705	1.117	347.0	0.667	1.500
280.1	0.697	1.139	347.5	0.680	1.601
281.7	0.708	1.135	347.6	0.680	1.696
		Sample VIII			
193.8	0.597	1.094	281.7	0.592	1.292
194.6	0.598	1.094	283.9	0.583	1.308
198.9	0.599	1.105	288.8	0.589	1.316
199.4	0.595	1.106	291.7	0.579	1.334
204.1	0.600	1.115	296.6	0.577	1.348
205.1	0.596	1.119	303.6	0.581	1.364
209.8	0.598	1.129	310.7	0.573	1.396
210.0	0.598	1.128	317.8	0.574	1.431
213.8	0.598	1.136	325.1	0.574	1.466
225.8	0.598	1.159	332.3	0.567	1.518
226.4	0.600	1.158	332.4	0.568	1.518

Table II (*Continued*)

t, °C	v', cm³	v'', cm³	t, °C	v', cm³	v'', cm³
231.5	0.603	1.168	339.8	0.563	1.600
239.1	0.602	1.187	343.5	0.562	1.684
241.8	0.596	1.194	345.8	0.576	1.770
249.1	0.597	1.210	346.2	0.575	1.814
259.2	0.592	1.237	346.8	0.577	1.896
265.0	0.591	1.249	347.0	0.559	1.940
272.8	0.589	1.273	347.5	0.571	2.116
280.2	0.584	1.297	347.6	0.575	2.173
		Sample IX			
193.7	0.514	1.210	284.1	0.506	1.435
194.6	0.513	1.212	288.8	0.508	1.445
199.0	0.516	1.218	291.7	0.504	1.458
199.4	0.515	1.221	296.2	0.506	1.467
204.2	0.519	1.227	296.6	0.499	1.479
205.1	0.522	1.224	303.6	0.502	1.523
209.9	0.514	1.243	310.7	0.499	1.533
210.0	0.519	1.241	317.8	0.497	1.568
213.8	0.516	1.251	325.1	0.496	1.612
225.9	0.518	1.274	332.3	0.489	1.675
226.4	0.522	1.273	332.4	0.490	1.673
231.5	0.531	1.279	339.8	0.485	1.779
239.1	0.520	1.301	343.5	0.485	1.883
241.9	0.513	1.313	345.7	0.496	1.988
249.1	0.514	1.332	346.2	0.503	2.034
259.2	0.518	1.352	346.8	0.503	2.136
265.1	0.513	1.371	347.0	0.491	2.192
272.8	0.506	1.398	347.5	0.496	2.350
280.2	0.510	1.418	347.6	0.497	2.405
		Sample X			
194.9	0.360	1.282	291.9	0.345	1.516
202.2	0.359	1.298	295.7	0.338	1.531
209.6	0.358	1.311	301.1	0.338	1.554
219.6	0.362	1.332	305.6	0.338	1.565
234.5	0.359	1.360	310.0	0.335	1.585
236.6	0.355	1.368	315.0	0.334	1.605
239.2	0.349	1.379	319.8	0.337	1.627
241.7	0.345	1.390	324.7	0.338	1.651
242.9	0.349	1.389	327.4	0.334	1.677
244.1	0.354	1.390	330.8	0.334	1.691
251.6	0.354	1.405	334.6	0.333	1.732
256.6	0.349	1.419	344.3	0.337	1.905
261.6	0.346	1.434	346.5	0.331	2.035
266.4	0.345	1.448	346.8	0.309	2.098
271.2	0.340	1.461	347.0	0.307	2.096
276.1	0.347	1.471	347.1	0.332	2.138
281.1	0.342	1.486	347.4	0.332	2.194
287.1	0.336	1.507	347.9	0.330	2.479

[a] Estimated uncertainty in temperature = ±0.5 °C. Estimated uncertainty in phase volumes = ±0.005 cm³.

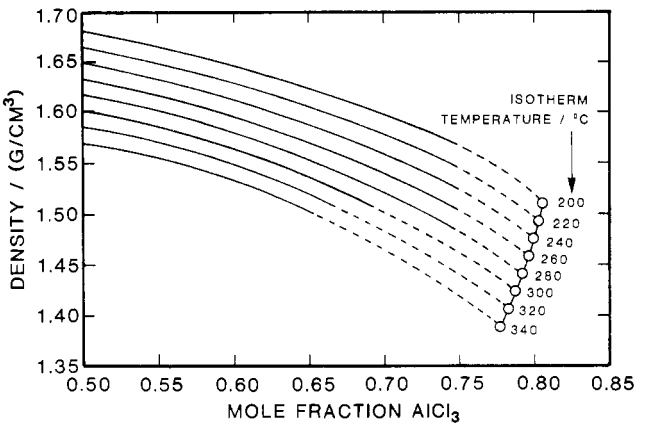

Figure 3. Densities of the single-liquid-phase region of $AlCl_3$–NaCl melt: (O) calculated from eq 5 and 6; solid lines on left from ref *1*.

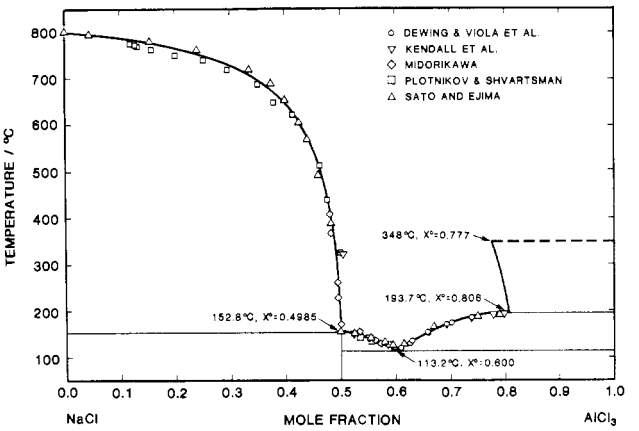

Figure 4. Phase diagram of the $AlCl_3$–NaCl binary system: (O) data of Viola et al. (*12*), treated by Dewing (*6*); (▽) Kendall et al. (*15*); (◇) Midorikawa (*16*); (□) Plotnikov and Shvartsman (*17*) and Shvartsman (*7*); (△) Sato and Ejima (*8*). X^0, t for monotectic and eutectic from Dewing (*6*), and for limits of liquid immiscibility line from present work and ref *3*.

$t \leq 340$ °C by first defining y' from eq 3, with the assumption that $y'' = 1.000$. These mole fractions were fitted to a cubic polynomial, given as eq 6. The standard deviation in X' was

$$X' = -0.1388 + (5.3192 \times 10^{-3})T - (9.6834 \times 10^{-6})T^2 + (5.6223 \times 10^{-9})T^3 \quad (6)$$

0.002. Equation 6 is plotted as the line of liquid–liquid immiscibility in Figure 4. As with eq 5, it appears that eq 6 can be safely extrapolated from 340 °C to the critical temperature, at which the upper liquid phase (i.e., pure $AlCl_3$(l)) disappears.

Figure 4 shows for the first time the complete phase diagram for the binary system $AlCl_3$–NaCl. Dewing (*6*) discusses critically the single-liquid-phase, $AlCl_3$-rich region, the equimolar region, and the slightly NaCl-rich region. His report probably is the most authoritative to date for these composition regions and is used as appropriate in Figure 4. The present study is the basis for the liquid–liquid immiscibility gap, as are data from Shvartsman (*7*) and Sato and Ejima (*8*) for the very basic region. It should be stressed that the liquid–liquid immiscibility line is the phase boundary when the system is subject to its own vapor pressure. This reaches values considerably higher than 1 atm. The critical temperature for the $AlCl_3$ liquid–vapor system will only be reached if $\rho_{av} = \rho_{crit}$. If ρ_{av} is less than this, the liquid $AlCl_3$ will disappear below the critical temperature, and a ρ_{av} greater than ρ_{crit} will result in the disappearance of the gaseous phase below the critical temperature.

The locus of eq 6 on a X,t diagram moves away from the $AlCl_3$ axis with increasing temperature and does not describe the typical dome generally observed for liquid–liquid immiscibility. The curvature is also opposite to what usually is found. As the appearance of this phase line is unusual, it is of interest to examine the thermodynamic implications of our findings.

The increasing region of immiscibility with increasing temperature (but not the curvature) may be straightforwardly understood from a species model (*9*) by assuming the presence of $AlCl_4^-$, $Al_2Cl_7^-$, and Al_2Cl_6 and a positive enthalpy change for the dissociation (*10*)

$$2Al_2Cl_7^- = 2AlCl_4^- + Al_2Cl_6 \quad (7)$$

Increasing temperature will increase the mole fraction of Al_2Cl_6. As the species model assumes that the pressure of Al_2Cl_6 is proportional to its mole fraction, the phase line will have to move toward lower X^0 to maintain the equilibrium with pure $AlCl_3$. The species model will be further discussed in a sub-

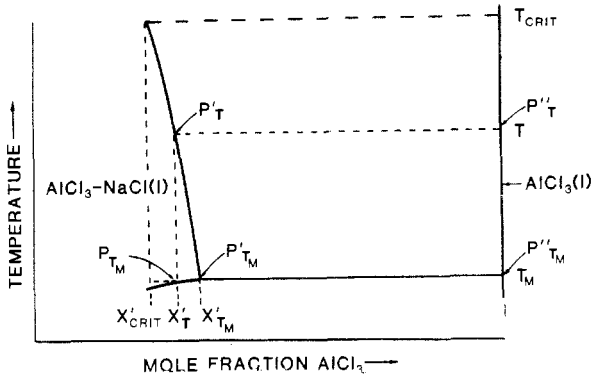

Figure 5. Liquid–liquid immiscibility gap for the $AlCl_3$–NaCl binary system.

sequent paper (*11*); here we will only outline a thermodynamic evaluation.

Refer to Figure 5 for a definition of the symbols used. P and a refer to Al_2Cl_6. The equilibrium condition for liquid–liquid phase separation may be expressed as

$$\ln (P'_T/P'_{T_M}) = \ln (P''_T/P''_{T_M}) \quad (8)$$

Introduction of P_{T_M} and activities at the constant temperature T_M gives

$$\ln (P'_T/P_{T_M}) + \ln (P_{T_M}/P'_{T_M}) = \ln (P''_T/P''_{T_M}) \quad (9)$$

or

$$\ln (P'_T/P_{T_M}) + \ln (a_{T_M}/a'_{T_M}) = \ln (P''_T/P''_{T_M}) \quad (10)$$

In view of the difference between the ionic melt, $AlCl_3$–NaCl, and pure $AlCl_3$(l), consisting only of Al_2Cl_6 molecules, it is reasonable to assume that the thermodynamics of vaporization of Al_2Cl_6 differs for the $AlCl_3$–NaCl melt and pure $AlCl_3$(l). The vaporization in either case is accompanied by a change in heat capacity, C_p.

A more consistent assumption would be to assume C_p for Al_2Cl_6(l) in the $AlCl_3$–NaCl phase to be constant, similar to what is given for $AlCl_3$(l) (*13*). A variable ΔC_p would result following the variation in C_p for Al_2Cl_6(g). The variation in ΔC_p was, however, only +5 J mol^{-1} K^{-1} over the total temperature range and is ignored in the present calculation. If for the $AlCl_3$–NaCl phase we assume ΔC_p to be constant in the temperature range of interest (466.85 $\leq T \leq$ 621.15 K) and ΔH_{T_M} to be independent of composition for the vaporization process

$$2AlCl_3(l)\ (\text{in } AlCl_3\text{–NaCl}) = Al_2Cl_6(g) \quad (11)$$

the following equation results

$$\frac{(\Delta H_{T_M} - \Delta C_p T_M)(T - T_M)}{RTT_M} + \frac{\Delta C_p}{R} \ln (T/T_M) = \ln (P''_T/P''_{T_M}) - \ln (a_{T_M}/a'_{T_M}) \quad (12)$$

where ΔH_T and ΔC_p refer to eq 11. This results because, if ΔC_p is constant, then

$$\Delta H_T = \Delta H_{T_M} + \int_{T_M}^{T} \Delta C_p \, dT$$

reduces to

$$\Delta H_T = \Delta H_{T_M} + \Delta C_p (T - T_M)$$

Using this ΔH_T in the Clausius–Clapeyron equation

$$\frac{d \ln P}{dT} = \frac{\Delta H}{RT^2}$$

gives on integration the form

$$\ln P = \frac{-\Delta H_{T_M}}{R}(1/T - 1/T_M) + \frac{\Delta C_p}{R} \ln (T/T_M) + \frac{\Delta C_p T_M}{R}(1/T - 1/T_M)$$

This equation gives

$$\ln P'_T = \frac{(\Delta H_{T_M} - \Delta C_p T_M)(T - T_M)}{RTT_M} + \frac{\Delta C_p}{R} \ln (T/T_M)$$

$$\ln P_{T_M} = 0$$

Substitution of these forms in a rearranged eq 10

$$\ln P'_T - \ln P_{T_M} = \ln (P''_T/P''_{T_M}) - \ln (a_{T_M}/a'_{T_M})$$

gives eq 12. In this derivation the influence of pressure on ΔH (difference in ΔH between the two liquid phases) has been neglected as

$$\int (\partial \Delta H/\partial P)_T \, dP = \int [\Delta v - T(\partial \Delta v/\partial T)_P] \, dP$$

is small relative to $\int \Delta C_p \, dT$ except very close to the critical point. Equation 12 permits the calculation of ΔH_T and ΔC_p if a_{T_M}/a'_{T_M} is known.

From the species model (*10*), which is based on vapor pressure data (*12*), we found that the activity of Al_2Cl_6 but not of $AlCl_3$ was proportional to X^0 in the present concentration range (0.777 $\leq X^0 \leq$ 0.806). The proportionality factor was 5.4. Hence, the activity of Al_2Cl_6

$$a_{T_M} = a'_{T_M}[1 + 5.4(X'_T - X'_{T_M})] \quad (13)$$

When pure liquid $AlCl_3$ is chosen as the standard state

$$a_{T_M} = 1 + 5.4(X'_T - X'_{T_M}) \quad (14)$$

The factor $X'_T - X'_{T_M}$ in eq 14 can be obtained from eq 6; i.e.

$$X'_T - X'_{T_M} = (5.3192 \times 10^{-3})(T - T_M) - (9.6834 \times 10^{-6})(T^2 - T_M^2) + (5.6223 \times 10^{-9})(T^3 - T_M^3) \quad (15)$$

The factor $\ln (P''_T/P''_{T_M})$ in eq 12 can be calculated from the JANAF Tables (*13*).

A least-squares fit of the experimental data to eq 12 yielded the values $\Delta H_{T_M} = 40.2 \pm 0.2$ kJ mol^{-1} and $\Delta C_p = -47.2 \pm 0.4$ J mol^{-1} K^{-1}. The corresponding values for vaporization of pure $AlCl_3$(l) are 39.7 kJ mol^{-1} and −80.3 J mol^{-1} K^{-1}, respectively (*13*). Only a small change in ΔH_{T_M} but a more substantial difference in ΔC_p for the two phases are needed to explain the experimentally observed phase separation line. This means that, although ΔH is only slightly lower for the $AlCl_3$ phase at temperature T_M, the enthalpy diminishes much more rapidly with temperature, the values being 32.9 and 27.7 kJ mol^{-1} for the $AlCl_3$–NaCl and the $AlCl_3$ phases, respectively, at the critical temperature. The difference in vaporization behavior of Al_2Cl_6 for the two phases is most likely attributed to anomalies in the $AlCl_3$ phase, the $AlCl_3$–NaCl phase showing more normal behavior. The $AlCl_3$ phase does approach the critical temperature in the actual temperature range,and weakening of bond forces to the Al_2Cl_6 molecules is expected to be more pronounced in this phase.

There have been some recently reported values for ΔC_p for $NaAlCl_4$ (*11*, *14*). If we, as Dewing (*6*), set the atomic C_p's to be equal, Dewing's value for an intermediate temperature (544 K) gives $\Delta C_p = -73.6$ J mol^{-1} K^{-1} and Roger's value yields $\Delta C_p = -60.7$ J mol^{-1} K^{-1}. Neither is as high as our −47.2 J

mol^{-1} K^{-1}, but both are higher values than given for pure $AlCl_3$(l).

The negative slope of the X',T curve can have unexpected implications in applications where one is working with $AlCl_3$–NaCl mixtures near the demixing compositions. A temperature rise of a sufficiently $AlCl_3$-rich melt could cause a phase separation which may not reequilibrate into a single phase upon cooling. It is kinetically difficult to transfer $AlCl_3$(l) into molten $AlCl_3$–NaCl without physically agitating the interface.

Safety

Appropriate precautions should be taken for the containment of liquids considerably above their normal boiling points in glass vessels. An especially dangerous situation can occur when $\rho_{av} > \rho_{crit}$ (see above). The gaseous phase will disappear above a certain temperature and the expansion of liquid $AlCl_3$ will then eventually result in rupture of the tube.

Acknowledgment

We thank Michael J. Dunn and Charles B. Hand for their interest and diligence when making all of the cathetometer readings.

Glossary

a	activity of Al_2Cl_6
C_p	heat capacity at constant pressure, J mol^{-1} K^{-1}
H	enthalpy, kJ mol^{-1}
m	mass, g
P	ideal gas pressure of Al_2Cl_6
t, T	temperature, °C and K, respectively
T_M	triple-point temperature of $AlCl_3$, 466.85 K
v	volume, cm^3
X	mole fraction $AlCl_3$, $AlCl_3$–NaCl scale
y	weight fraction $AlCl_3$, $AlCl_3$–NaCl scale
ρ	density, g cm^{-3}
^{0}, $'$, $''$, $'''$	superscripts denoting overall sample, $AlCl_3$–NaCl phase, $AlCl_3$(l) phase, and $AlCl_3$(g) phase, respectively

Literature Cited

(1) Fannin, A. A., Jr.; Kibler, F. C., Jr.; King, L. A.; Seegmiller, D. W. *J. Chem. Eng. Data* **1974**, *19*, 266.
(2) King, L. A.; Seegmiller, D. W. *J. Chem. Eng. Data* **1971**, *16*, 23.
(3) Viola, J. T.; Seegmiller, D. W.; Fannin, A. A., Jr.; King, L. A. *J. Chem. Eng. Data* **1977**, *22*, 367.
(4) Seegmiller, D. W.; Fannin, A. A., Jr.; Olson, D. S.; King, L. A. *J. Chem. Eng. Data* **1972**, *17*, 295.
(5) Johnson, J. W.; Cubicciotti, D.; Silva, W. J. *High Temp. Sci.* **1971**, *3*, 523.
(6) Dewing, E. W. *Metall. Trans., B* **1981**, *12*, 705.
(7) Shvartsman, Yu. I. *Zap. Inst. Khim., Akad. Nauk Ukr. RSR* **1940**, *7*, 3.
(8) Sato, Y.; Ejima, T. *Nippon Kinzoku Gakkaishi* **1978**, *42*, 905.
(9) Øye, H. A.; Rytter, E.; Klaeboe, P.; Cyvin, S. J. *Acta Chem. Scand.* **1971**, *25*, 559.
(10) Øye, H. A., Universitetet i Trondheim, Trondheim, Norway, unpublished data, 1981.
(11) Fannin, A. A., Jr.; King, L. A.; Øye, H. A., United States Air Force Academy, unpublished data, 1981.
(12) Viola, J. T.; King, L. A.; Fannin, A. A., Jr.; Seegmiller, D. W. *J. Chem. Eng. Data* **1978**, *23*, 122.
(13) "JANAF Thermochemical Tables", 2nd ed.; *Natl. Stand. Ref. Data Ser. (U.S., Natl. Bur. Stand.)* **1971**, *No. 37*.
(14) Rogers, L. J. *J. Chem. Thermodyn.* **1980**, *12*, 51.
(15) Kendall, J.; Crittenden, E. D.; Miller, H. K. *J. Am. Chem. Soc.* **1923**, *45*, 963.
(16) Midorikawa, R. *Denki Kagaku* **1955**, *23*, 72.
(17) Plotnikov, V. O.; Shvartsman, Yu. I. *Zap. Inst. Khim., Acad. Nauk Ukr. RSR* **1936**, *3*, 387.

Received for review December 11, 1980. Accepted November 2, 1981.

Equilibrium Phase Properties of Selected *m*-Xylene Binary Systems. *m*-Xylene–Methane and *m*-Xylene–Carbon Dioxide

Heng-Joo Ng, Sam S.-S. Huang, and Donald B. Robinson*

Department of Chemical Engineering, University of Alberta, Edmonton, Alberta, Canada T6G 2G6

Vapor and liquid equilibrium phase compositions have been measured at 310.9, 394.3, and 477.6 K for the *m*-xylene–methane binary system and at 310.9, 338.7, 394.3, and 477.6 K for the *m*-xylene–carbon dioxide system. At each temperature, the pressure ranged from the vapor pressure of *m*-xylene to about 15 MPa, although in the case of the *m*-xylene–carbon dioxide system, pressures were extended to the vicinity of the critical region at about 17 MPa. The data were used to calculate equilibrium ratios for each component in the binary system.

Introduction

In order to predict the behavior of typical natural gas condensate and other systems containing heavier undefined fractions of interest to the gas processing industry, it is necessary to have information on the binary pairs making up the mixtures. This is particularly true when the system contains nonparaffinic hydrocarbons and nonhydrocarbons such as carbon dioxide, hydrogen sulfide, or nitrogen. Successful modeling of the behavior of these complex mixtures requires good information on the pure compounds and on the binary interactions that exist between the different molecular species.

The recent work of Ng and Robinson (*1*, *2*) on toluene–carbon dioxide, methylcyclohexane–carbon dioxide, and methylcyclohexane–hydrogen sulfide and Kalra et. al. (*3*) on *n*-heptane–carbon dioxide binary systems represented part of a continuing program to measure the properties of typical light hydrocarbons or nonhydrocarbons with C_{7+} binaries. In this study, two systems containing *m*-xylene were studied. Equilibrium vapor and liquid phase compositions in the *m*-xylene–methane system were measured at three temperatures ranging from 311 to 478 K and pressures from the vapor pressure of *m*-xylene to about 15 MPa. In the *m*-xylene–carbon dioxide system the measurements were made at four temperatures ranging from 311 to 478 K and pressures from the vapor pressure of *m*-xylene to the vicinity of the critical region at each temperature. This range of temperature overlaps slightly the temperatures studied for this system in the recent work of Sebastian et al. (*4*), who made experimental phase composition measurements at four temperatures from 463 to 583 K. The measured phase compositions were used to calculate the

0021-9568/82/1727-0119$01.25/0